Eur. Phys. J. A **4**, 61–68 (1999)

THE EUROPEAN PHYSICAL JOURNAL A

Analysis of proton-induced reactions on ^{208}Pb with incident energy 590 MeV and 322 MeV

Fan Sheng[1], Li Zhuxia[1,2], Zhao Zhixiang[1], Ding Dazhao[1]

[1] China Institute of Atomic Energy, P.O.Box 275(41), Beijing 102413, China
[2] Institute of Theoretic Physics, Academia Sciences, P.O.Box 2735, Beijing 100080, China

Received: 16 January 1998 / Revised version: 17 September 1998
Communicated by W. Weise

Abstract. The double differential cross section of emitting particles, the mass and charge distribution of the residual nuclei from proton-induced reaction on ^{208}Pb with incident energy 590 MeV and 322 MeV have been analyzed by the quantum molecular dynamics (QMD). The time scale of the change of reaction mechanism in the process of reaction is investigated. The reaction process can be divided into three stages i.e., the direct, the cascade and the evaporation stage with the corresponding time scale of about <30 fm/c, 30–100 fm/c and >100 fm/c, respectively.

1 Introduction

Recently, the research for the energy generation and waste transmutation by using intermediate energy proton accelerator driven radiologically clean nuclear system(ADS) [1,2,3,4] has attracted considerable attention. ADS consists of three parts: accelerator, spallation target and subcritical reactor. The spallation neutron source induced by intermediate energy proton-nucleus interaction is an important link for transmutation and applications. The detailed knowledge of the target material, such as the double differential cross section and the spectrum of emitting particle, the neutron yield and the energy deposited when bombarded by incident proton beam etc., is needed for ADS. The mass and charge distribution of residual products produced in the spallation reaction also needs to be studied because it can provide useful information for the disposal of nuclear waste and residual radioactivity generated by the system.

The quantum molecular dynamics (QMD) model [5,6,7,8] has been applied to heavy- and light-ion induced reactions rather successfully. The model was used for the analysis of the double differential cross section of (p, xn) and (p, xp) reactions in [9–12] and it was proposed that for nucleon-nucleus collisions with the energy well above Coulomb barrier up to several GeV, the whole reaction process could be divided into two parts, the dynamical process and statistical process, and these two processes are well separated in their time scales. In the dynamical process, the direct reaction, cascade reaction and dynamical formation of highly-excited fragments take place during typical collision time of the order of 10^{-22} second. And after dynamical process, the evaporation and fission occur. This stage is called the statistical process which can be treated by statistical decay model (SDM). Then one parameter t_{sw}, the switching time from the QMD calculation to SDM, has to be introduced. In [10], $t_{sw} \sim 100$ fm/c was adopted. By using QMD plus SDM and adjusting the switching time t_{sw}, the calculation results of the double differential cross section (p, xn) and (p, xp) reactions were in reasonable agreement with the measured data. The residual nuclear fragment formation cross section for 1.5 GeV p + 56Fe was investigated in [14] by the same model and switching time and the experimental data were reproduced well. However, a switching time from QMD to SDM has to be put in by hand. Differently, in this work we do not introduce the artificial switching to SDM but extend the time of QMD calculation to longer time until the particle emission ends. We pay special attention to the preparation of stable initial nuclei. The time scale of the cascade process in the intermediate energy nucleon-induced reaction was studied based on the average kinetic energy of two colliding nucleons in their center of mass system and it was pointed out to be about 20 fm/c [13]. We will use our model to study the time scale of the change of the reaction mechanism in the reaction process. It can provide the necessary reference for the switching time from QMD to SDM.

^{208}Pb is considered to be one of the prospective target material in ADS. Therefore, the study of the reactions of intermediate energy proton bombarding ^{208}Pb is of great interest. In this work we perform a systematic investigation of the reactions of 590 MeV and 322 MeV proton beam on ^{208}Pb. The double differential cross section (p, xn) and (p, xp), the mass and charge distribution of residual nuclear fragments are analyzed and compared

with experimental data. The experimental measurement for that reaction was done by Filges [15], Summerer's [16] and Gloris [17] etc.

The paper is organized as follows: In Sect. 2, we briefly introduce the model as well as the parameters used. In Sect. 3 we present our calculation results and detailed comparisons with experimental data as well as the empirical formula. In Sect. 4, a summary and discussion are given.

2 The QMD model and the properties of the ground state

2.1 The QMD model

In QMD model, each nucleon is represented by a Gaussian wave packet in both the coordinate and momentum space in the following way,

$$f_i(\vec{r},\vec{p},t) = \frac{1}{\pi\hbar^3}\exp\left(-(\vec{r}-\vec{r}_i(t))^2/2L^2\right) \times\exp\left(-(\vec{p}-\vec{p}_i(t))^2 2L^2/\hbar^2\right), \quad (1)$$

where L is a parameter which represents the spatial spread of wave packet, $\vec{r}_i(t)$ and $\vec{p}_i(t)$ denote the center of the wave packet in the coordinate and momentum space, respectively.

Integrating over momentum space yields the distribution in coordinate space,

$$f_i(\vec{r},t) = \int \frac{d\vec{p}}{(2\pi\hbar)^3} f_i(\vec{r},\vec{p},t) = \frac{1}{(2\pi L)^{3/2}}\exp\left[-(\vec{r}-\vec{r}_i(t))^2/2L^2\right], \quad (2)$$

and the baryon density is

$$\rho(\vec{r},t) = \sum_{i=1}^{N} f_i(\vec{r},t). \quad (3)$$

The equation of motion for $\vec{r}_i$ and $\vec{p}_i$ is given, ($i = 1,\ldots,N$, N is the number of particles) by the Newtonian equations

$$\dot{\vec{r}}_i = \frac{\partial H}{\partial \vec{p}_i}$$
$$\dot{\vec{p}}_i = -\frac{\partial H}{\partial \vec{r}_i}, \qquad i = 1,\ldots,N \quad (4)$$

The effective nucleon-nucleon interaction includes Skyrme, Yukawa, Coulomb,symmetry energy and the momentum dependent interaction. The Pauli potential is adopted to simulate the Pauli effect in the particle propagation.

$$V_i = V^{loc}+V^{Yuk}+V^{Coul}+V^{Sym}+V^{MDI}+V^{Pauli}, \quad (5)$$

$$V^{Loc} = t_1\delta(\vec{r}_1-\vec{r}_2)+t_2\delta(\vec{r}_1-\vec{r}_2)\delta(\vec{r}_1-\vec{r}_3), \quad (6)$$

$$V^{Yuk} = v^{Yuk}\frac{\exp\{|\vec{r}_1-\vec{r}_2|\}/a\}}{|\vec{r}_1-\vec{r}_2|}, \quad (7)$$

$$V^{Coul} = \frac{1}{4}\frac{e^2}{|\vec{r}_1-\vec{r}_2|}(c_i+1)(c_j+1) \quad (8)$$

$$V^{Sym} = C_s c_i c_j \delta(\vec{r}_1-\vec{r}_2) \quad (9)$$

$$V^{MDI} = t_4\ln^2[t_5(\vec{p}_1-\vec{p}_2)^2+1]\delta(\vec{r}_1-\vec{r}_2), \quad (10)$$

$$V^{Pauli} = v_p\left(\frac{\hbar}{p_0 q_0}\right)^3 \exp\{-(\vec{r}_1-\vec{r}_2)^2/2q_0^2\} \times\exp\{-(\vec{p}_1-\vec{p}_2)^2/2p_0^2\}, \quad (11)$$

where t_1, t_2, t_4, t_5 are parameters, the symmetry energy coefficient is taken to be 34 MeV and c_i is 1 for proton and -1 for neutron. For the infinite symmetric nuclear matter the above interaction (5–11) potential reads as

$$U(\rho) = \alpha\left(\frac{\rho}{\rho_0}\right)+\beta\left(\frac{\rho}{\rho_0}\right)^{\gamma}+\delta\ln^2\left\{1+\varepsilon\left(\frac{\rho}{\rho_0}\right)^{2/3}\right\}\frac{\rho}{\rho_0}. \quad (12)$$

The parameters adopted in this work are listed in Table 1.

In the QMD model, the stochastic two-body collision process is introduced in a phenomenological way on the test-particle calculation of the BUU scatting term [18]. We adopt a parametrization of N-N cross section which is similar to that of Niita [10]. The parametrization nucleon-nucleon elastic cross section is adopted:

$$\sigma = \frac{D_1}{1+100\sqrt{s'}}+D_2 \text{ (mb)} \quad (13)$$

with

$$\sqrt{s'} = \max(0,\sqrt{s}-M_i-M_J-cutoff) \text{ (GeV)} \quad (14)$$

where M_i is the i'th scatting nucleon mass (in GeV) and is the energy of the collision nucleons i'th and j'th at the center-of-mass system. The cutoff is 0.2 GeV for nucleon-nucleon channel, while it is zero for the others. We use this form up to $\sqrt{s'} = 0.4286$ GeV, which corresponds to 1 GeV Lab energy for nucleon-nucleon case. Above 1 GeV, we parametrize the experimental p-p and p-n elastic cross section as:

$$\sigma = D_3\left[1-\frac{2}{\pi}\tan^{-1}(1.5\sqrt{s'}-0.8)\right]+D_4 \text{ (mb)} \quad (15)$$

where D_1, D_2, D_3 and D_4 are the parameters whose values are taken from [10].

2.2 The properties of ground state

An important ingredient of QMD calculation is how to make initial nuclei stable within the time scale interested in. It means that we should prepare the initial nuclei to

Table 1. Parameters used in the calculations

α	β	γ	ν^{Yuk}	a	v_p	q_0	p_0	L	ρ_0
−116 MeV	76 MeV	2	−5 MeV	1.2 fm	17 MeV	6 fm	60 MeV/c	2.0 fm	0.168 fm^{-3}

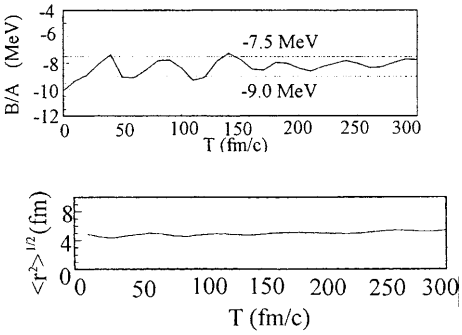

Fig. 1. The Time evolution of binding energy and root mean square radius of initial nuclei

be close to "ground state". In addition to fulfilling the static properties of ground state such as the binding energy and the root mean square radius, the evolution of those quantities should be stable enough and the behavior of the density and momentum distribution should be approximately correct. Therefore we take the following initialization procedure for ^{208}Pb: First, the position of each nucleon in nucleus is sampled by Woods-Saxon distribution, then the momentum of each nucleon is sampled within a local Fermi sphere based on local density approximation. After the sampling we make a pre-selection that is that only the system for which the energy is within the range of $E_{bin} \pm 0.5$ MeV is taken as a candidate for further selection. For pre-selected system, we make further tests i.e., we let the system evolutes with time according to the equation motion (4) until 300 fm/c. Only the system for which the binding energy, the root mean square radius, the behavior of the density and momentum distribution keep smooth variation and without spurious particle emission are finally selected. We select 20 initial nuclei of ^{208}Pb from 10000 prepared nuclear systems and then store up them for using in the QMD calculations.

Figure 1 shows the time evolution of the binding energy and root mean square radius of initial nuclei. We observe that they fluctuate around the mean values (7.5–8.5 MeV/n for binding energy and 5.4 fm for root mean square radius). The small fluctuation is due to the fact these nuclei still have a small excitation energy. However, as one can see that the initial nuclei are keeping stable within the period of 300 fm/c. Figure 2 shows the time evolution of the density distribution of prepared ^{208}Pb. The solid histogram denotes the QMD simulation and the line is calculated by the empirical theory. They are in consistency. We see a quite smooth density distribution within the period of 300 fm/c, and the nuclei selected remain stable.

The average momentum distribution for prepared ^{208}Pb is shown in Fig. 3. The solid histogram is obtained by QMD simulation. The line is the empirical distribution parametered by a super-position of two Gaussians [19].

$$\rho(p) = c\{\exp(-p^2/p_0^2) + \varepsilon_0 \exp(-p^2/q_0^2)\},$$
$$p_0 = \sqrt{2/5}\, p_F,\ q_0 = \sqrt{3}\, p_0,\ \varepsilon_0 = 0.07, \qquad (16)$$

where c is a normalization constant and p_F is the Fermi momentum. We see that they are in agreement. It means that the momentum distribution of prepared nuclei is suitable.

In this work, the time step is chosen to be 1 fm/c, and the total time is 300 fm/c. After 300 fm/c, we find the particle emission process is stopped. Of course the residual nuclei decay process still continue mainly via gamma-rays emission and fission. In this work, the gamma-rays emission and fission are not considered and they are unimportant for the (p, xn) and (p, xp) reactions. For the limitation of our computer CPU, 500 events are selected.

3 Numerical results

We have studied the reactions $p + {}^{208}$Pb at $Ep = 590$ Mev and 322 MeV. The range of the impact parameter b varies from 0 to 9 fm which is selected slightly bigger than the nuclear radius of ^{208}Pb. The double differential cross section can be written as

$$\frac{d^2\sigma}{dEd\Omega} = \int_0^{b_{max}} 2\pi b g(b, E, \Omega) db, \qquad (17)$$

where b is the impact parameter, b_{max} is the maximum value of impact parameter, $g(b, E, \Omega)$ denotes the average multiplicity of the particle (neutron, proton, Δ, etc.) emitted in unit energy-angular interval around E and for the events with impact parameter b.

The residual nuclear fragment formation cross section can be written as

$$\sigma = \int_0^{b_{max}} 2\pi b q'(b) db, \qquad (18)$$

where $g'(b)$ denotes the average multiplicity of the fragment concerned for the events with impact parameter b.

Figure 4 shows the energy spectra of emitting particles, Fig. 4a is for the case of the impact parameter $b = 0.1$ fm. For this case, we find that the solid histogram is divided into three parts, corresponding to the direct, cascade and evaporation processes by two large steps. And the two large steps result from the change of reaction mechanism at the energy region of high, medium and low. The spectrum of emitting particles with impact parameter $b = 6$ fm is given in Fig. 4b. At the high energy part, a large jump is shown for this case. It is due to the fact that the

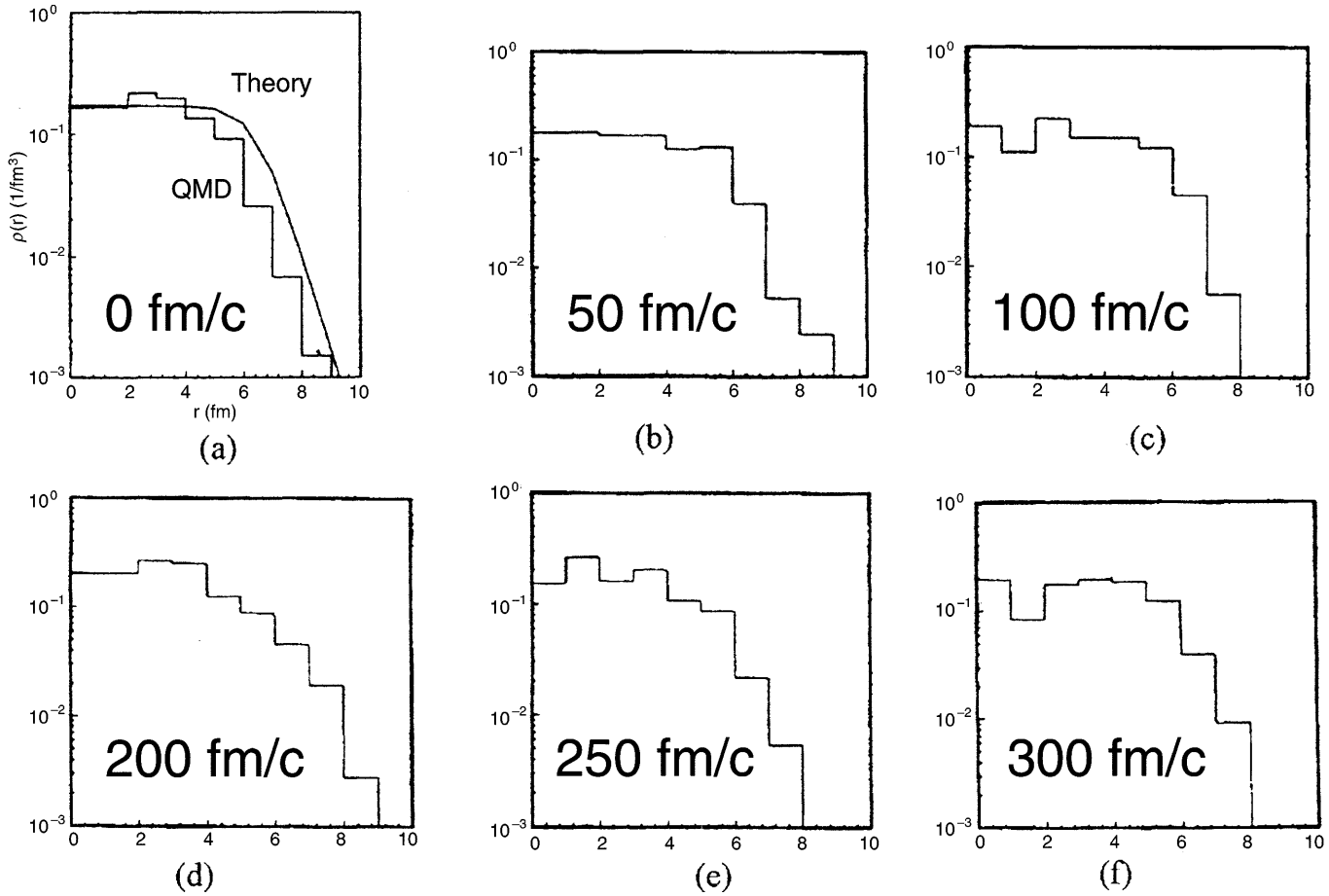

Fig. 2. a–f. The time evolution of density distribution of prepared ^{208}Pb

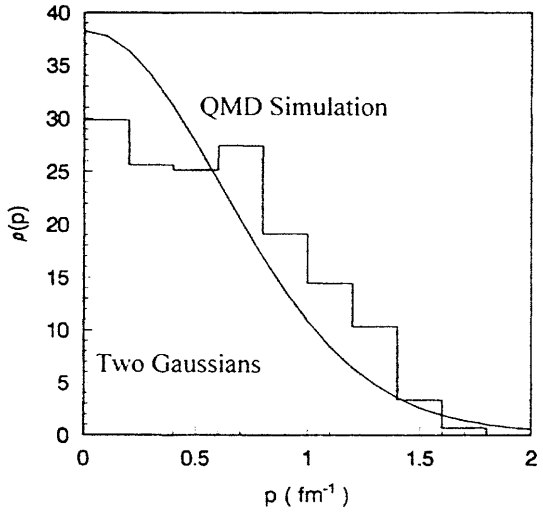

Fig. 3. The average momentum distribution for prepared ^{208}Pb

incident proton may pass through the target directly since the impact parameter almost approaches the nuclear radius where the density is low and therefore the emitting proton energy reduces only due to the Coulomb scattering.

In order to study the change of the reaction mechanism we further show the time evolution of the average multiplicity of the particle emitted in the unit energy in Fig. 5. Again three parts, corresponding to direct, cascade and evaporation process, divided by two minimums are exhibited. The change of the slope denotes the change of the reaction mechanism. The two minimums are caused by competing between the different mechanism. The direct and cascade processes competing happen at about 30 fm/c, and the cascade and evaporation processes competing at 100 fm/c. The time scale obtained here is similar to that of S. Chiba [13] and K.Niita[10]. In Fig. 4, we find that the number of emitting particles at the energy region of 30–110 MeV for impact parameter $b = 0.1$ fm case is much higher than that of $b = 6$ fm. And correspondingly in Fig. 5, the first minimum for the impact parameter $b = 6$ fm case is much deeper than that of $b = 0.1$ fm. It is because for $b = 6$ fm case, the impact parameter is close to the nuclear radius the grazing reaction happens, and therefore the contribution from the cascade process is highly reduced.

In the Fig. 6 we show the double differential cross sections for ^{208}Pb(p, xn) with incident energy 590 MeV for laboratory angles $\theta = 30°$, $\theta = 90°$, and $\theta = 150°$, respectively. The solid-histogram denotes the results of

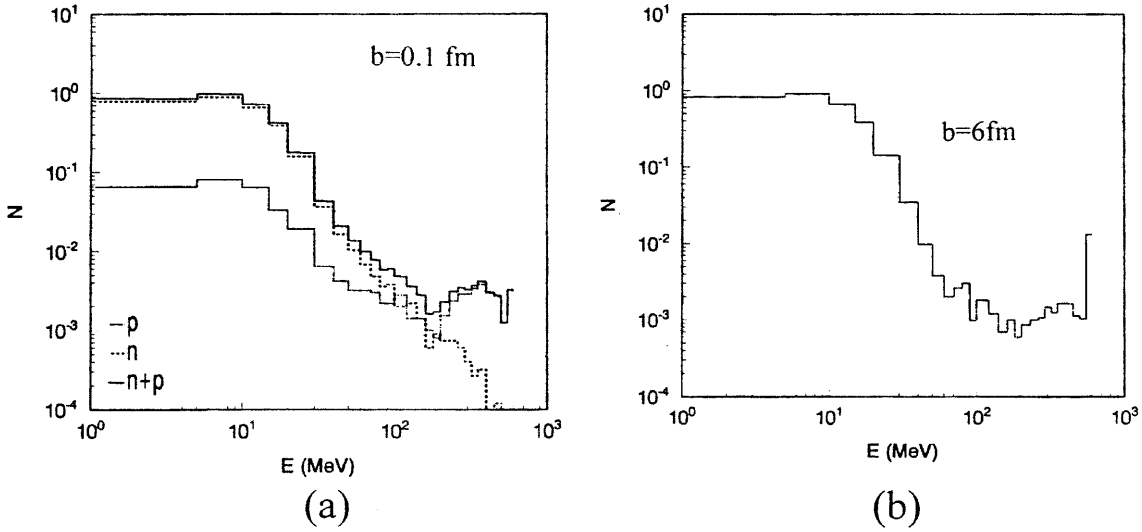

Fig. 4.a,b. The energy spectra of emitting particles with impact parameter $b = 0.1$ fm and $b = 6$ fm, respectively

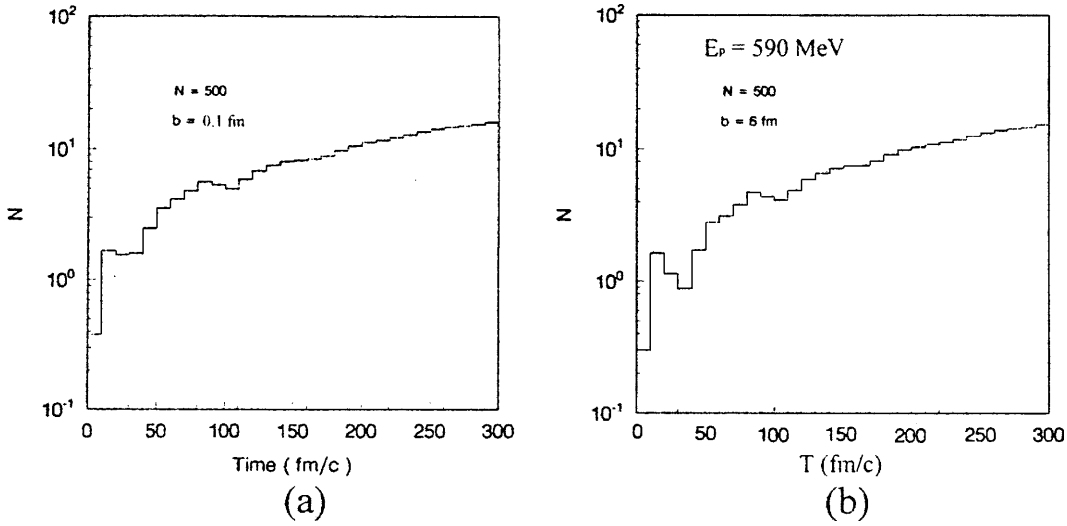

Fig. 5.a,b. The time evolution of multiplicity of the particle emission in the unit energy

QMD simulation, the open squares denote the experimental data [15]. Generally, the experimental data are reasonably reproduced by the QMD calculations. For $\theta = 90°$, $\theta = 150°$, the results obtained by QMD simulation are in good agreement with the experimental measurement, but for $\theta = 30°$, we find the deviations from the measurement data i.e. calculation results for high energy part are lower than experimental data.

Figure 7 gives the QMD prediction of the double differential cross section of ^{208}Pb(p, xp) reaction with incident energy $Ep = 590$ MeV at the laboratory angular $\theta = 30°$, and $\theta = 150°$. We find that there exists a big jump in the spectra at the emitting proton energy $Ep > 300$ MeV. The reason is understood as the incident proton may pass through the target for the large impact parameter case and then the grazing reaction happens.

The residual nuclear fragment mass and charge distribution are investigated. For the present QMD model calculations, the fission process is not included, and therefore, the results obtained by QMD calculation are only the spallation products. The residual nuclear fragment formation cross section with $Z = 81$ and $A = 190$ is shown in Fig. 8a,b. The dots denote the QMD simulation and the lines denote the K.Summerer's empirical formula [16]. We find that typical spallation residual nuclear products are in the vicinity of the target. Fig. 8a shows the mass distribution of residual nuclei with $Z = 81$, when $A < 191$ side, the results of QMD reproduce the K. Summerer's empirical formula well, however, at $A < 191$ side, the production yield of QMD prediction is larger than that of empirical formula. As the K. Summerer's empirical formula was obtained by parameterizing the experimental data measured by radiochemical method, only the nuclear fragments having considerable long life time can be measured. So it is reasonable that the QMD prediction are higher than experimental data at $A < 191$ side since the nuclei of $Z = 81$ and $A < 191$ side are very neutrons deficient and therefore very unstable. Fig. 8b shows the charge distribution

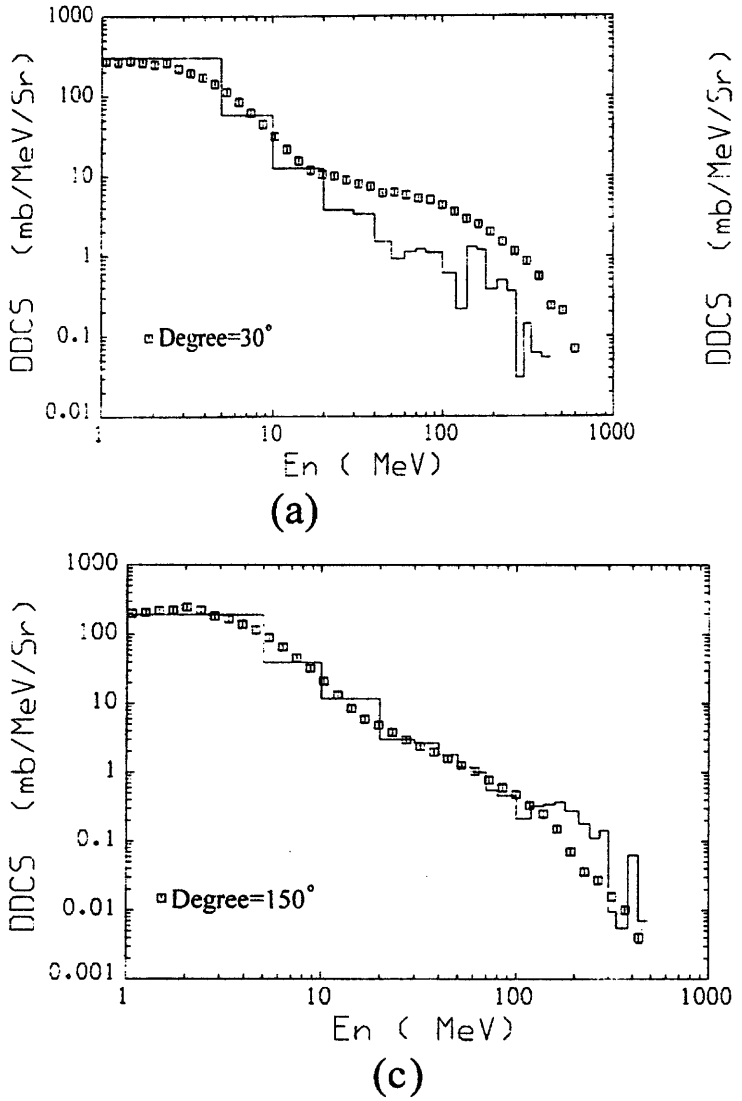

Fig. 6. a–c. The double differential cross sections for ^{208}Pb(p, xn) at angular $\theta = 30°$, 90° and 150° in the lab. system. The solid histogram denotes the QMD calculation results and the open squares denote the measurement [15]

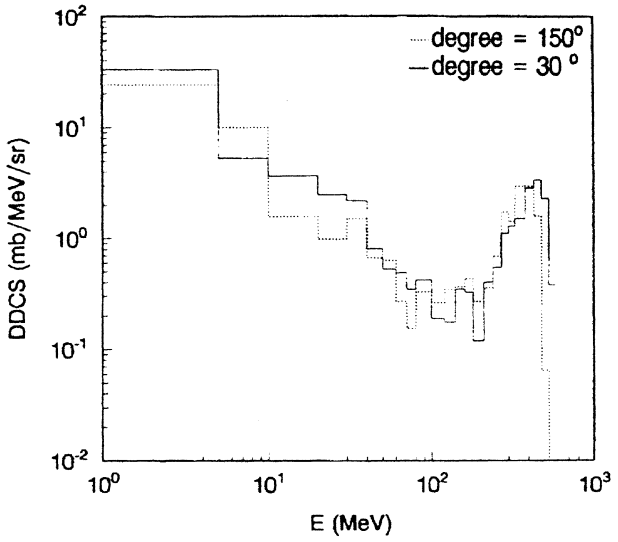

Fig. 7. The double differential cross section of (p,xp) reaction with the incident proton energy $Ep = 590$ MeV

of residual nuclei with $A = 190$. In this case, the fragments with $Z \geq 81$ are very proton rich and unstable, consequently the prediction of QMD simulation is higher than that of K. Summerer's empirical formula.

Figure 9 shows the mass distribution of residual nuclear fragments of 322 MeV proton bombarding ^{nat}Pb. The solid circles are the results of QMD simulation. The open squares are the experimental data [17] and the line is the results of K. Summerer's formula. Fig. 9a gives a survey of the cross section over the covered range of the masses of production with the proton incident energy $Ep = 322$ MeV bombarding natural Pb. Two regions of product nuclides can be clearly distinguished. The fission products locate approximately at the half of the mass of the target while the typical spallation products are in the vicinity of the target. Since the fission process has not been taken into account in the present QMD calculations and the calculation results are only the spallation products. The calculations including fission products should be studied in the future work. As far as the spallation products are concerned, the prediction is in good agreement

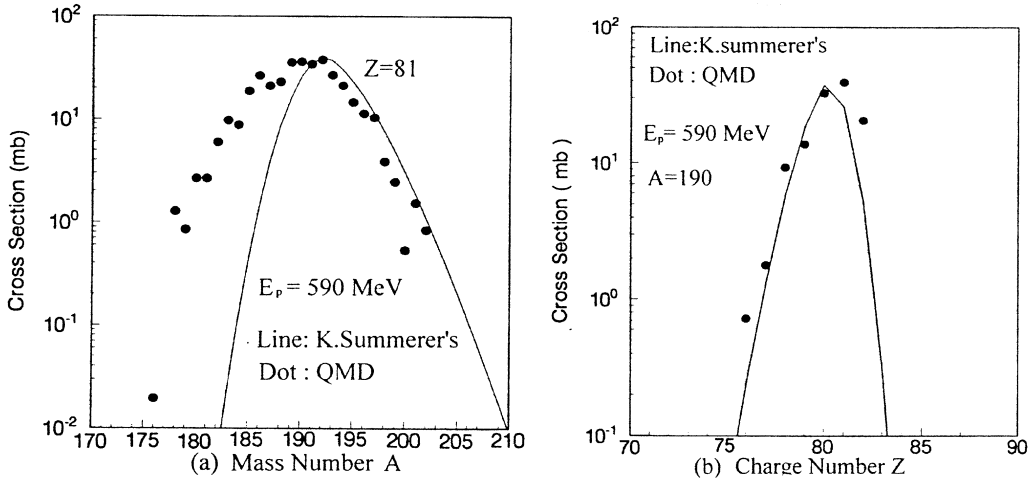

Fig. 8. a, b. The mass and charge distribution of the residual nuclear fragments of $Z = 81$ and $A = 190$ respectively.The dots denote the QMD calculation, and the line is obtained from K. Summerers empirical formula [16]

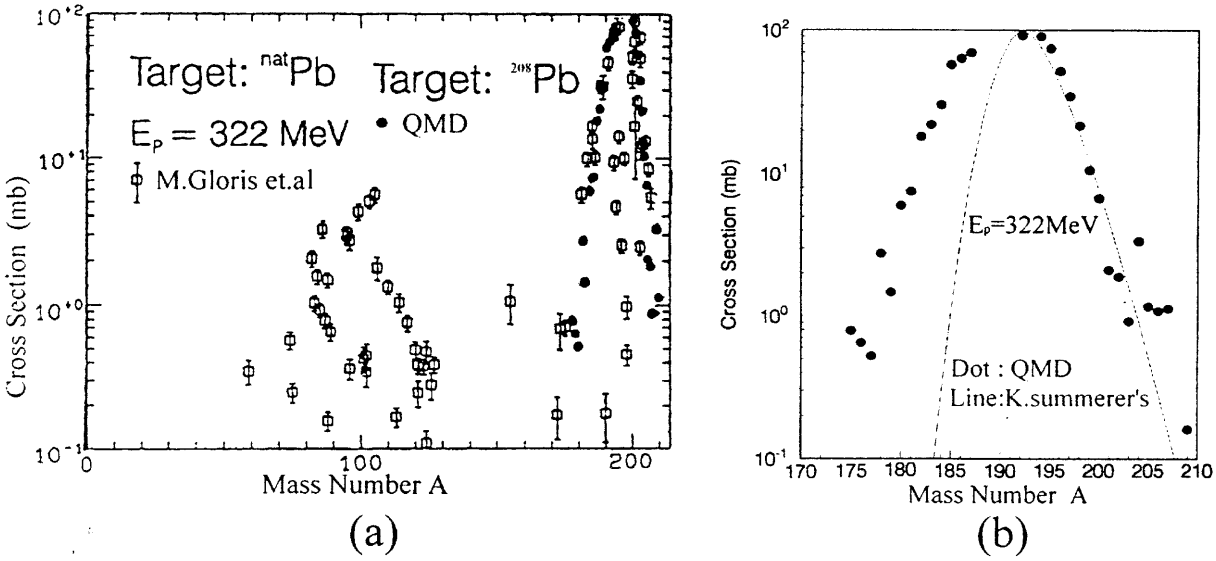

Fig. 9. a, b. Mass distribution of the residual nuclear fragments with the incident proton energy $Ep = 322$ MeV. The solid circles are the results of QMD simulation.The open squares are measured data [17] and the line is the K. Summerer's formula [16]

with the measured data. Figure 9b is shown the results obtained by QMD simulations (dot denoted) compared with the results of K. Summerer's empirical formula(line denoted). We find again on the neutron-deficient side the QMD prediction is higher than the empirical formula.

4 Summary and discussion

In this work, we have studied the the reactions at $Ep =$ 590 MeV and 322 MeV by QMD calculations. The double differential cross section of (p, xn) and (p, xp) reactions, mass and charge distribution of the residual nuclei are analyzed. The theoretical predictions are in reasonable agreement with experimental data as well as the empirical formula of mass and charge distribution of residual nuclei. The further study for improvement of the deviation from the data of double differential cross section (p, xn) at forward angle for high energy part of spectrum and the calculation of including the fission products should be considered in the future work.

Furthermore, we have also studied the emitting particle spectra and the time evolution of the multiplicity of emitting particle in order to study the reaction mechanism. We find that for the center collisions, the reaction process can be divided into three stages i.e., the direct, the cascade and the evaporation, the corresponding time scale is about <30 fm/c, 30–100 fm/c and >100 fm/c, respectively.

As the impact parameter increases the contribution from the cascade process is reduced. For the peripheral reaction, the cascade process contribution becomes much

suppressed due to the geometrical limitation. Our studies indicate the QMD model is a useful approach for the intermediate energy proton induced reaction and gains an advantage than the cascade plus evaporation model that needs a lot of adjustable parameters.

The work is supported by the National Natural Science Foundation of China under contract N0. 19675069. Fan Sheng, one of the authors, would like to thank the China Nuclear Data Center (CNDC) for providing their workstation.

References

1. C.D. Bowman et.al.: Nucl. Instr. And Meth. In Phys. Res. **A320**, 336 (1992)
2. C. Rubbia et.al.: CERN/AT/95-44(ET)
3. T. Mukaiyama et.al.: IAEA,TCM,Madrid,Sept. 17–19, (1997)
4. Zhao Zhixiang et. al.: Second International Conference on Accelerator-Driven Transmutation Technologies and Applications, Kalmar, Sweden, (1996)
5. J. Aichelin et.al.: Phys. Reports, **202**, No. 5&6, 233 (1991)
6. C. Hantnack et.al.: Nucl. Phys. **A495**, 303 (1989)
7. J. Aichelin et.al.: Phys. Rev. **C37**, 2451 (1988)
8. T.C. Sangster et.al: Phys. Rev. **C46**, 1404 (1992)
9. G. Peilert et.al.: Phys. Rev. **C46**, 1457 (1992)
10. K. Niita et.al.: Phys. Rev. **C52**, 2620 (1995)
11. M.B. Chadwick et.al.: Phys. Rev. **C52**, 2800 (1995)
12. S. Chiba et.al.: Phys. Rev. **C53**, 1824 (1996)
13. S. Chiba et.al.: Phys. Rev. **C54**, 3302 (1996)
14. S. Chiba et.al.: Phys. Rev. **C54**, 285 (1996)
15. D. Filges et.al: KFK-3779 (1980)
16. K. Summerer et.al.: Phys. Rev. **C42**, 2546 (1990)
17. M. Gloris et.al: NEA/NSC/DOC(97) 13 (1997)
18. G. F.Bertsch and S.Das Gupta: Phys. Rep. **160**, 189 (1988)
19. Y. Haneishi et.al.: Phys. Rev. **C33**, 260 (1986)